Journal of Power Sources 243 (2013) 65–71

Contents lists available at SciVerse ScienceDirect

Journal of Power Sources

journal homepage: www.elsevier.com/locate/jpowsour

Graphene-based non-noble-metal Co/N/C catalyst for oxygen reduction reaction in alkaline solution

Kexing Niu [a,b], Baoping Yang [b], Jinfeng Cui [b], Jutao Jin [a], Xiaogang Fu [a], Qiuping Zhao [b], Junyan Zhang [a,*]

[a] State Key Laboratory of Solid Lubrication, Lanzhou Institute of Chemical Physics, Chinese Academy of Sciences, Lanzhou 730000, PR China
[b] School of Petroleum Chemical Engineering, Lanzhou University of Technology, Lanzhou 730050, PR China

HIGHLIGHTS

- Polyethyleneimine (PEI) was used as nitrogen source in the catalyst synthesis for the first time.
- Graphene-based Co/N/rGO(NH_3) as high-performance cathode catalyst for oxygen reduction reaction in alkaline solution.
- Graphene-based Co/N/rGO catalytic activity is better than the single N/rGO or heat-treatment in Ar one.
- Similar catalytic activity as Pt/C towards ORR in alkaline solution.

GRAPHICAL ABSTRACT

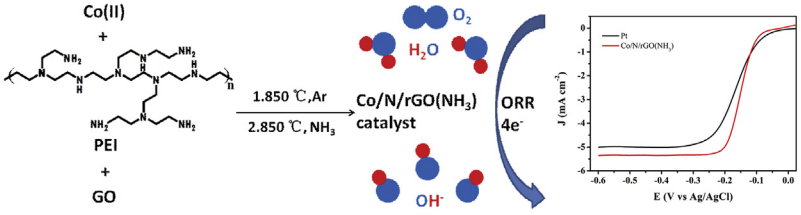

ARTICLE INFO

Article history:
Received 3 April 2013
Received in revised form
3 June 2013
Accepted 3 June 2013
Available online 12 June 2013

Keywords:
Non-noble-metal catalyst
Oxygen reduction reaction
Graphene
Cobalt
Alkaline

ABSTRACT

This study develops a promising catalyst for oxygen reduction reaction (ORR) via a simple two-step heat treatment of a mixture of cobalt(II) nitrate hexahydrate ($Co(NO_3)_2 \cdot 6H_2O$), polyethyleneimine (PEI), and graphene oxide (GO), firstly in argon atmosphere and then in ammonia atmosphere. X-ray photoemission spectroscopy (XPS) result reveals that the catalyst has pyridinic N-dominant (46% atomic concentration among all N components) on the surface. The kinetics measurement of the catalyst in 0.1 M KOH solution using a rotating disk electrode (RDE) reveals that the catalyst (Co/N/rGO(NH_3)) has high activity. Furthermore, the number of electrons exchanged during the ORR with the catalyst is determined to be ~3.9, suggesting that the ORR is dominated by a $4e^-$ reduction of O_2 to H_2O. The catalyst has good stability, and its performance is superior to the commercial Pt/C(20%) catalyst in alkaline condition, making the material a promising substitute to noble metal ORR electrocatalyst on the cathode side of fuel cells.

1. Introduction

Fuel cells have a tremendous attraction to researchers because it is a clean, efficient, and dependable source of energy, and are expected to become more widely employed in the near future [1]. The use of electrocatalysts with high loading of Pt or Pt-alloys in the electrode, leads to high cost which hinders further commercialization and market acceptance of fuel cells [2]. Considering high cost and low abundance of Pt, a lot of research efforts have been focused on the development of non-noble metal catalysts (NNMCs) to replace Pt for catalyzing oxygen reduction reaction (ORR) [3,4].

For NNMCs catalysts, carbon-supported transition metal/nitrogen (M/N/C, M = Co, Fe, Mn, *etc.*) materials have gained increased attention due to their promising catalytic activity towards the ORR. In comparison with the other carbon materials, such as carbon nanotubes, graphite nanofibers, activated carbons, graphene

* Corresponding author. Tel./fax: +86 (0)9314968295.
E-mail address: zhangjunyan@licp.cas.cn (J. Zhang).

0378-7753/$ – see front matter © 2013 Elsevier B.V. All rights reserved.
http://dx.doi.org/10.1016/j.jpowsour.2013.06.007

possesses unique physical properties such as high specific surface areas [5], superior electric conductivities [6], and excellent mechanical strength and elasticity [7]. All these properties make graphene a highly promising electrocatalyst support. A series of graphene-based nanomaterials were rationally designed, such as N-doped graphene, graphene/metal oxides, and other graphene-based nanomaterials, they all showed enhanced activity and stability for ORR, comparable to the commercial Pt/C catalyst under alkaline conditions [8]. On the other hand, proper M–N_x (where x is the coordination number of N atoms to metal) structure is of great concern in the pursuit of M/N/C catalysts with high performance. One critical factor determining the ORR activity of M/N/C catalysts is found to be the pyridinic nitrogen content. Although, many sources of N have recently been used to improve pyridinic nitrogen content to form M–N_x sites on carbon surface [9–14], the pyridinic nitrogen content is not high enough. When the catalyst precursor is pyrolyzed under NH_3 stream, the resultant catalysts have higher microporosities and pyridinic nitrogen contents. The higher microporous surface in the catalysts is capable of enhanced catalytic activity [15], since transition metal could coordinate easily with nitrogen to form M–N_x structure as highly active site to facilitate ORR performance.

In this paper, a graphene-based high nitrogen content oxygen reduction NNMC was synthesized for the first time, we introduced Co–N_x moieties into graphene by annealing treatment of a mixture of $Co(NO_3)_2 \cdot 6H_2O$, polyethyleneimine (PEI), and graphene oxide (GO), first in argon and second in ammonia to afford the Co/N/rGO(NH_3) electrocatalyst. The morphology of the catalyst was characterized by scanning electron microscope (SEM) and transmission electron microscopy (TEM). The surface element and nitrogen content were characterized by X-ray photoelectron spectroscopy (XPS). The electrocatalytic activities for oxygen reduction were then investigated by cyclic voltammetry (CV) and rotating disk electrode (RDE) in alkaline solutions. The durability was investigated by chronoamperometric measurement. The results of the Co/N/rGO(NH_3) catalyst were compared with that of the commercial Pt/C(20%) to assess the potential use as the cathode catalyst for fuel cells.

2. Experimental

2.1. Sample preparation

2.1.1. Graphene oxide synthesis

Graphene oxide (GO) was made using an improved method reported by Marcano [16]. Briefly, 3 g of raw graphite powder (100 mesh) was added to a mixture of H_2SO_4 360 mL and H_3PO_4 40 mL in flask, then 12 g $KMnO_4$ was added into flask slowly in ice-bath to keep the reaction temperature below 45 °C. The flask was then heated in an oil bath at 50 °C and vigorous stirring for 12 h. The reaction mixture was cooled to room temperature and poured onto ice (600 mL) with 30% H_2O_2 solution (60 mL). The suspension was stirred at room temperature for 10 min. It was then centrifuged (5000 rpm for 5 min), and the supernatant was decanted away. The remaining solid material was then washed in sequence with 200 mL of water, 200 mL of 3% HCl, and 200 mL of anhydrous ethanol (EtOH), respectively. The material remaining after multiple-wash process was coagulated with 200 mL of ether, and the resulting suspension was filtered over a PTFE membrane with a 0.45 μm pore size. The solid obtained on the filter was vacuum-dried overnight at room temperature.

2.1.2. Catalysts synthesis

GO powder was sonicated (100 W for 1 h) dispersed in deionized water, the concentration of the GO water suspension was 1.67 mg mL^{-1}. The first step in the preparation of typical Co/N/GO, 30 mg of $Co(NO_3)_2 \cdot 6H_2O$ was added in 50 mL polyethyleneimine (PEI) aqueous solution (10 mg mL^{-1}), and stirred for 30 min. Then 150 mL of GO suspension was added with vigorous stirring for 12 h at room temperature in order to prevent an inhomogeneous mixing. After that, the mixture from the first step was transferred to the vacuum freeze dryer, and freezed for 24 h. Finally, the resulting product (Co/N/GO) was transferred from the beaker to the gas tube furnace. The temperature of tube furnace was elevated to 850 °C at 4 °C min^{-1} of ramping rate and ~100 cc min^{-1} of Ar gas flow and held at 850 °C for 120 min, which was then cooled to room temperature, and the step also reduced GO to rGO (denoted as Co/N/rGO(Ar)). The product was acid-leached in 0.5 M H_2SO_4 at 85 °C for 8 h to remove any unstable and ORR-nonreactive phases, and thoroughly washed in deionized water 3 times [17,18]. The preleached catalyst then underwent a second heat treatment in NH_3 atmosphere as the final step of the synthesis. The temperature of tube furnace was elevated to 850 °C at 4 °C min^{-1} of ramping rate and ~400 cc min^{-1} of NH_3 gas flow and held at 850 °C for 30 min (denoted as Co/N/rGO(NH_3)).

2.2. Physical characterizations

The surface morphologies and size of sample were investigated using field emission SEM (Hitachi S-4800) and TEM (Teanai-G2-F30). SEM and TEM samples were prepared by drop-drying sample from their anhydrous ethanol suspension onto silicon substrates and copper grids, respectively. XPS was performed on an Axis Ultra (Kratos, Manchester, UK). For the excitation of the photoelectron spectra Al Kα ($h\nu$ = 1.4867 keV) was used. We used a hemispheric analyzer working at a pass energy of 20 eV for N 1s core level and Co 2p core levels. All spectra were calibrated by setting the C 1s photo emission peak for sp^2-hybridized carbons to 284.8 eV and were fitted after a Shirley type back ground subtraction.

2.3. Electrochemical measurements

Four milligrams of catalyst powder was dispersed in mixture of 750 μL of deionized water, 210 μL of ethanol, 40 μL of Nafion (5 wt% solution in a mixture of lower aliphatic alcohols and water, Aldrich). The mixture was sonicated 100 W for 3 h to form a homogeneous ink, and kept in a sealed vial. Then 5 μL of catalyst ink was dropped on a glassy carbon (GC) electrode of 3 mm in diameter (0.071 cm^2 of geometric area) and was dried for 12 hours at room temperature. On the basis of the ink composition, a total catalyst loading mass on the GC electrode was ~20 μg, which corresponded to a loading amount of 0.28 mg cm^{-2} on the basis of the geometric area of GC.

Cyclic voltammetry and rotating disk voltammetry were conducted at room temperature with a μAUTOLABIII potentiostat in a three-electrode electrochemical cell using the sample modified GC electrode as the working electrode, a Pt wire as the counter electrode, and a saturated silver chloride electrode (Ag/AgCl) as the reference electrode. Electrolyte was saturated with oxygen before the start of every experiment by bubbling O_2 at least 15 min, which was maintained over the electrolyte in order to ensure its continued O_2 saturation during the recording. The working electrode was cycled at least 20 times before data were recorded at a scan rate of 50 mV s^{-1} from +0.1 to −0.60 V vs. Ag/AgCl in O_2 saturated 0.1 M KOH solution.

3. Results and discussion

3.1. Structural characterization

As shown in Fig. 1, XPS results of the Co/N/rGO(NH_3) sample provide evidence for the incorporation of Co and N into the rGO, which is used to correlate the electrochemical activity of the catalyst with their chemical composition. XPS survey-scan

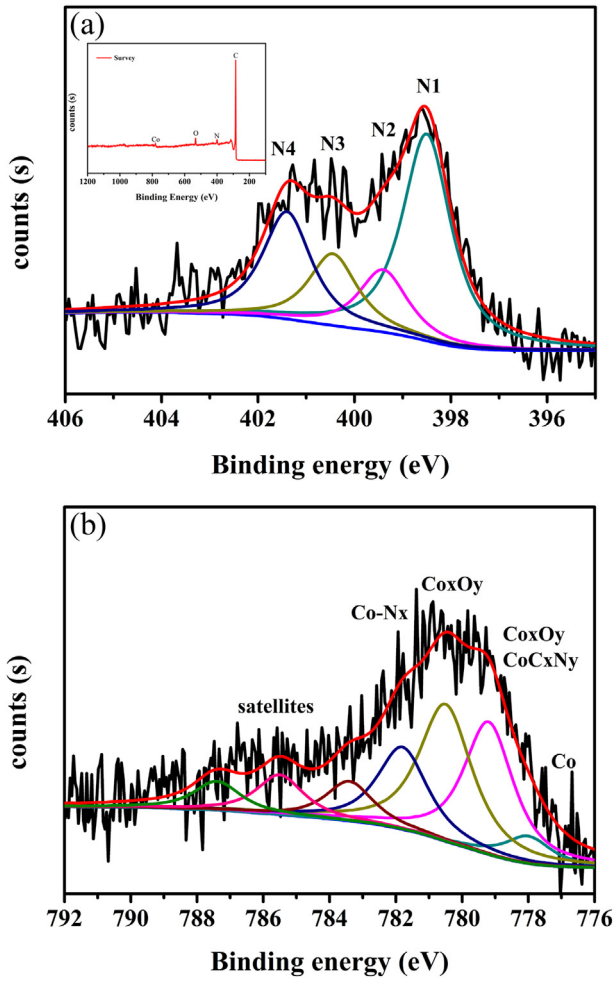

Fig. 1. (a) Decomposed XPS N1s binding energy spectra of Co/N/rGO(NH_3) catalyst (inset shows the survey scan spectrum), (b) decomposed XPS Co 2p binding energy spectra of Co/N/rGO(NH_3) catalyst.

spectrum shows C1s, N1s, O1s and Co 2p in the Co/N/rGO(NH_3) (inset in Fig. 1a). The XPS N1s spectrum reveals the presence of (1) pyridinic N (398.5 eV) [19], (2) nitrile N and Co–N_x (399.4 eV) [20], (3) pyrrolic N (400.5 eV) [19], and (4) quaternary N (401.4 eV, protonated pyridine or graphitic-N) [19] (Fig. 1a). Most of oxygen-containing functional groups derived from the GO were eliminated after the first heat treatment in Ar [21]. The atomic ratios of N, O and Co relative to C of the Co/N/rGO(NH_3) sample are ~0.068, 0.021, and 0.007, respectively. As shown in Table 1, the relative N content is high when the sample was heated via two-step heat treatment. Note that pyridinic N among all N components has the highest concentration (46 at.%). Interestingly, this Co/N/rGO(NH_3) catalyst, shows a high fraction of pyridinic N than N-containing graphene prepared by post-treatment of GO with NH_3 gas annealing [22] which had shown mainly quaternary N.

The heat treatment step is required for the formation of the active sites for ORR, at high temperature, the Co metal particle will produce, and the size will be reduced with the higher temperature [20]. The Co/N/rGO(Ar) sample was preleached in 0.5 M H_2SO_4 to remove any unstable phases so as to make more active sites be exposed. However, as shown in Fig. 1b, the Co peak did not disappear in XPS spectrum after the acid-washing. It is possible that the Co nanoparticle was surrounded by some materials which are not decomposed in acid. The metal and nitrogen associated to the rGO-support may create new carbon structures enriched in nitrogen and metal.

Table 1
Ratio analysis of the peaks in XPS spectra in Co/N/rGO(NH_3) catalyst.

Sample	% C	% O	% Co	%N				
				N total	N1	N2	N3	N4
Co/N/rGO(NH_3)	91.2	1.91	0.66	6.23	46.15	13.94	15.98	23.93

Because pyridinic N and pyrrolic N both can coordinate with Co [23,24], it is possible that the nitrile groups (reported at 399.4 ± 0.2 eV) [20] present in the form of associated with cobalt in Co–N_x structures in the binding energy range of N2 at the high temperature. The XPS results confirm the formation of Co–N_x moieties into the graphene sheets. In addition, the decomposition of Co 2p XPS spectrum (Fig. 1b) gives three main peaks for Co–N and one metallic Co peak, the peak at 781.8 eV is due to the cobalt associated with N in Co–N_x structures [25], which is consistent with the corresponding peak detected in the N 1s spectrum (N2), the two peaks at 780.4 eV and 779 eV correspond to a mixture of cobalt oxides [26]. In other words, XPS data further confirm the presence of Co metallic particles (at 778 eV), found in SEM and TEM images (Fig. 2), and amounts of cobalt oxides in the Co/N/rGO(NH_3) sample. As shown in Fig. 2(a) and (b), it can be seen that many nanoparticles are formed and uniformly distributed on the graphene surface after a two-step heat treatment. Fig. 2(c) and (d) shows the Co nanoparticles are like core coated with graphene sheets, the diameter of the Co nanoparticle is about 20 nm. It is possible that this special core/shell structure could play an important role in the electrocatalysis processes.

3.2. Electrochemical measurements

The catalytic activity of the Co/N/rGO(NH_3) material to ORR was evaluated at first by cyclic voltamperometry (CV) in N_2-saturated (black curve) and O_2-saturated (red curve) 0.1 M KOH at a scan rate of 50 mV s^{-1} from +0.1 to −0.60 V vs. Ag/AgCl at first, respectively (Fig. 3). It can be seen that the voltammograms of Co/N/rGO(NH_3) is essentially featureless in the N_2-saturated electrolyte, while that exhibits a significant oxygen reduction peak potential (E_{ORR}) at 0.24 V and the corresponding current density of ca. 9.5 mA cm^{-2} in the O_2-saturated electrolyte. The results strongly indicate that the Co/N/rGO(NH_3) catalyst possesses excellent electrocatalytic activity for the ORR (For interpretation of the references to color in this paragraph, the reader is referred to the web version of this article.).

The role of the second heat treatment in NH_3 to the catalytic activity of Co/N/rGO(NH_3) catalyst was investigated by evaluating a NH_3-free controlled sample, by only heat treatment a Co/N/GO mixture at 850 °C in argon atmosphere (denoted as Co/N/rGO(Ar)). The ORR activity of Co/N/rGO(Ar) was measured by CV in an alkaline medium that E_{ORR} = −0.193 V vs. Ag/AgCl was obtained as a result, much lower than that of Co/N/rGO(NH_3) (Fig. 4a). This suggests that NH_3 has a significant effect on improving the ORR catalytic activity. To gain deeper insight into the ORR process, RDE measurements were further carried out to study ORR activity on these catalysts in the O_2-saturated 0.1 M KOH solution at a scanning rate 5 mV s^{-1}. Fig. 4b shows the ORR polarization curves of Co/N/rGO(Ar) and Co/N/rGO(NH_3) at a rotation rate of 1600 rpm. As expected, the onset potential for oxygen reduction at the Co/N/rGO(NH_3) electrode is substantially more positive than that at the Co/N/rGO(Ar) electrode. When sample was pyrolyzed under NH_3 atmosphere, due to the etching effect of NH_3, the resultant Co/N/rGO(NH_3) catalyst has higher microporosities and pyridinic nitrogen content than only Ar-pyrolyzed Co/N/rGO(Ar) catalyst. Microporosity created upon pyrolysis and pyridinic nitrogen contents are

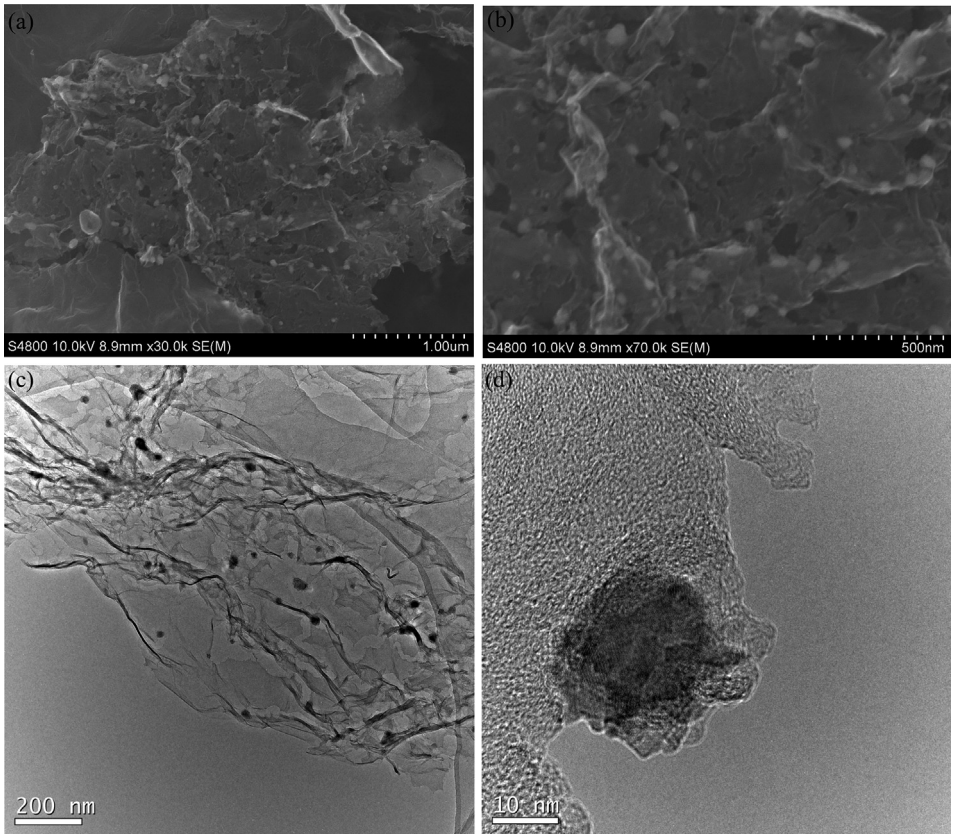

Fig. 2. SEM and TEM images of Co/N/rGO(NH_3). (a) and (b) SEM images of Co/N/rGO(NH_3) powder. (c) Low-resolution and (d) high-resolution TEM image of a Co particle phase on the catalyst surface.

important factors for ORR activity, which is supported by the better ORR performance of NH_3-pyrolyzed catalysts compared to Ar-pyrolyzed catalysts [27,28].

The role of the cobalt in the catalytic activity of Co/N/rGO(NH_3) catalyst was investigated by evaluating a cobalt-free controlled sample as a comparison, annealed a N/GO mixture at 850 °C first in argon atmosphere and second in NH_3 atmosphere (denoted as N/rGO(NH_3)). The ORR activity of N/rGO(NH_3) was measured by CV in an alkaline medium that $E_{ORR} = -0.310$ V vs. Ag/AgCl was obtained,

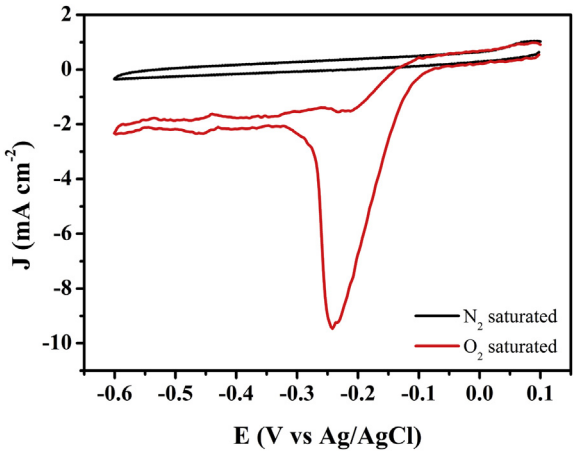

Fig. 3. Cyclic voltammograms of Co/N/rGO(NH_3) catalyst. Electrolyte: N_2-saturated (black curve) and O_2-saturated (red curve) 0.1 M KOH, scan rate: 50 mV s^{-1}, and catalyst loading: 280 μg cm^{-2} (For interpretation of the references to color in this figure legend, the reader is referred to the web version of this article.).

much lower than that of Co/N/rGO(NH_3) (Fig. 4c). This suggests that cobalt has a significant effect on improving the ORR catalytic activity. The RDE measurements were further carried out to study ORR activity of these catalysts in the O_2-saturated 0.1 M KOH solution at a scanning rate 5 mV s^{-1}. Fig. 4d shows the ORR polarization curves of N/rGO(NH_3) and Co/N/rGO(NH_3) at a rotation rate of 1600 rpm. As expected, the onset potential for oxygen reduction at the Co/N/rGO(NH_3) electrode is substantially more positive than that at the N/rGO(NH_3) electrode.

Based on above results, it is clear that compared with the role of cobalt, the pyridinic N is found to be the dominant component in Co/N/rGO(NH_3) catalyst, higher content of pyridinic N could easily form defect complexes with carbon vacancies in the graphene, four pyridinic N atoms and a divacancy would form a porphyrin-like rectangular defect complex. It has also suggested that the rectangular porphyrin-like rectangular defect in graphene fits very well for a metal ion (Π), resembling the Co-porphyrin-like molecule [29]. Based on the high percentage of the pyridinic N and the presence of Co—N peak in the XPS analysis, we conclude that Co—N_x moieties could be formed into the graphene sheets. The high electrocatalytic ORR activity of Co/N/rGO(NH_3) can be attributed to the higher incorporation of pyridinic N and Co into the graphene sheets.

These experiments not only demonstrate that the second heat treatment in NH_3 atmosphere can improve the ORR catalytic activity markedly, but also emphasizes that the Co plays a key role in the catalytic performance of Co/N/rGO(NH_3) catalyst by forming various Co-based species that either contribute effectively as active species, or only apply some local electronic effects on the N-containing sites. Moreover, we propose that cobalt associated with nitrogen in Co—N_x structures may be a component of the catalytic active site towards the ORR.

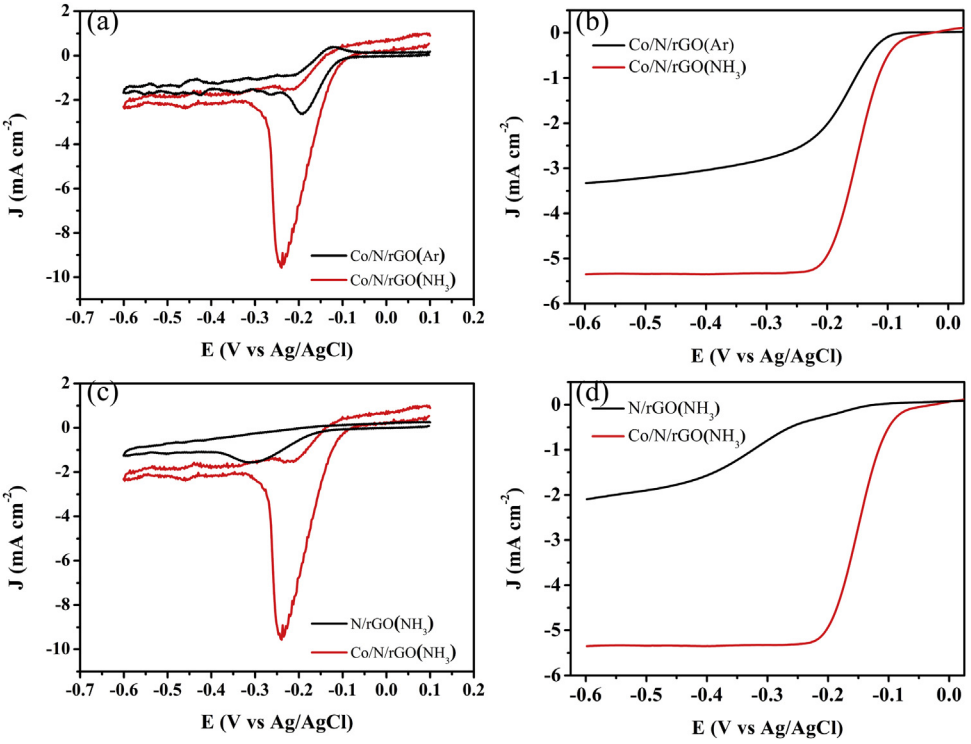

Fig. 4. Cyclic voltammograms of samples. (a) Co/N/rGO(NH_3) (red curve) and Co/N/rGO(Ar) (black curve), (b) Co/N/rGO(NH_3) (red curve) and N/rGO(NH_3) (black curve). Electrolyte: O_2-saturated 0.1 M KOH, scan rate: 50 mV s^{-1}, and catalyst loading: 280 μg cm^{-2}. RDE voltammograms of samples. (c) Co/N/rGO(NH_3) (red curve) and Co/N/rGO(Ar) (black curve), (d) Co/N/rGO(NH_3) (red curve) and N/rGO(NH_3) (black curve). Electrolyte: O_2-saturated 0.1 M KOH, scan rate: 5 mV s^{-1}, electrodes rotating 1600 rpm, and catalyst loading: 280 μg cm^{-2} (For interpretation of the references to color in this figure legend, the reader is referred to the web version of this article.).

The electrocatalytic activity and kinetic parameters of Co/N/rGO(NH_3) to ORR were investigated by using a thin-film rotating disk electrode (RDE) in O_2-saturated 0.1 M KOH at a scan rate of 5 mV s^{-1} from +0.1 to −0.60 V vs. Ag/AgCl over a range of rotation rates from 400 to 2400 rpm. Linear sweep voltammograms (LSV) recorded for the Co/N/rGO(NH_3) catalyst and Pt/C(20%) catalyst (Fig. 5(a) and (b)) show an increase in the catalytic current density with rotation rate. The increased current density could be attributed to the decrease of interface concentration polarization between electrolyte and electrode with the increase of the rotating rate. The diffusion-limited current is higher for commercial Pt/C(20%) catalyst. The catalytic activity of Co/N/rGO(NH_3) exhibits a well-defined limiting plateau which implies the ORR is diffusion-controlled below −250 mV. The ORR is under diffusion-kinetic control at higher potential (from −250 to −160 mV), and is current independent in the range from −160 to −50 mV controlled by the charge-transfer kinetics.

For the oxygen reduction on an RDE, Koutecky–Levich plots (J vs. $\omega^{1/2}$) were analyzed at different electrode potentials. The slopes of their best linear fit lines were used to calculate the number of electros transferred (n) on the basis of the Koutecky–Levich equation.

$$\frac{1}{J} = \frac{1}{J_L} + \frac{1}{J_K} = \frac{1}{B\omega^{1/2}} + \frac{1}{J_K} \quad (1)$$

$$B = 0.62nFC_0D_0^{2/3}\nu^{-1/6};\ J_K = nFkC_0 \quad (2)$$

where J is the measured current density, J_K and J_L are the kinetic and diffusion-limiting current density, respectively, ω is the electrode rotation rate, n is transferred electro number, F is the Faraday constant, C_0 is the O_2 saturation concentration of the electrolyte, ν is the kinematic viscosity of the electrolyte, D_0 is the O_2 diffusion coefficient of the electrolyte, and k is the electro-transfer rate constant. In the Koutecky–Levich plots, $(J)^{-1}$ is the y-axis, $\omega^{1/2}$ is the x-axis, and $(J_K)^{-1}$ indicates the intercept.

Diffusion-limited current densities collected at different rotation rates in the potential range from −0.50 to −0.30 V vs. Ag/AgCl were used to determine the number of electrons transferred associated with ORR, the overall current density (J^{-1}) was plotted against the square root of angular velocity ($\omega^{1/2}$). Fig. 6(a) and (b) depicts the corresponding Koutecky–Levich (K–L) plots for Co/N/rGO(NH_3) catalyst and Pt catalyst, respectively. Based on Eqs. (1) and (2), the number of electron transfer in oxygen reduction (n) of the Co/N/rGO(NH_3) was estimated to be 3.9, which is comparable to other non-noble metal catalysts for the four-electron ORR; for example, $n = 3.9$ for N-doped carbon nanotubes [3], $n = 2.8 \sim 3.5$ for N or S-doped graphene [30], $n = 3.7$ for B/N-doped CNTs [31], $n = 3.89$ for nitrogen-doped ordered mesoporous graphitic arrays [32], and $n = 3.89$ for MnO_2/C [33]. In addition, the kinetic-limiting current density was calculated to be $J_K = 18.9$ mA cm^{-2} at −0.5 V, higher than that of commercially Pt–C/GC ($J_K = 5.1$ mA cm^{-2} at −0.5 V) [30], S–G ($J_K = 3.3$–5.3 mA cm^{-2} at −0.5 V) and N–G ($J_K = 2.5$–7.8 mA cm^{-2} at −0.5 V) [30], N-CNT ($J_K = 5.37$–9.53 mA cm^{-2} at −0.5 V) [34], and BN-CNT ($J_K = 10.13$ mA cm^{-2} at −0.3 V) [31], which further confirms the high ORR performance of Co/N/rGO(NH_3).

A characteristic two polarization curves for the ORR are displayed in Fig. 7 to have a benchmark of the electrocatalytic properties of Co/N/rGO(NH_3) against Pt/C(20 wt%), the same amount of catalysts by mass (280 μg cm^{-2}) was loaded onto a GC RDE at 1600 rpm. High diffusion-limited current was due to the high number and uniform distribution of ORR active sites on the surface of catalyst [35]. The significant feature of Co/N/rGO(NH_3) catalyst is the positive shift of the onset potential for ORR, E_{onset} (−110 mV vs.

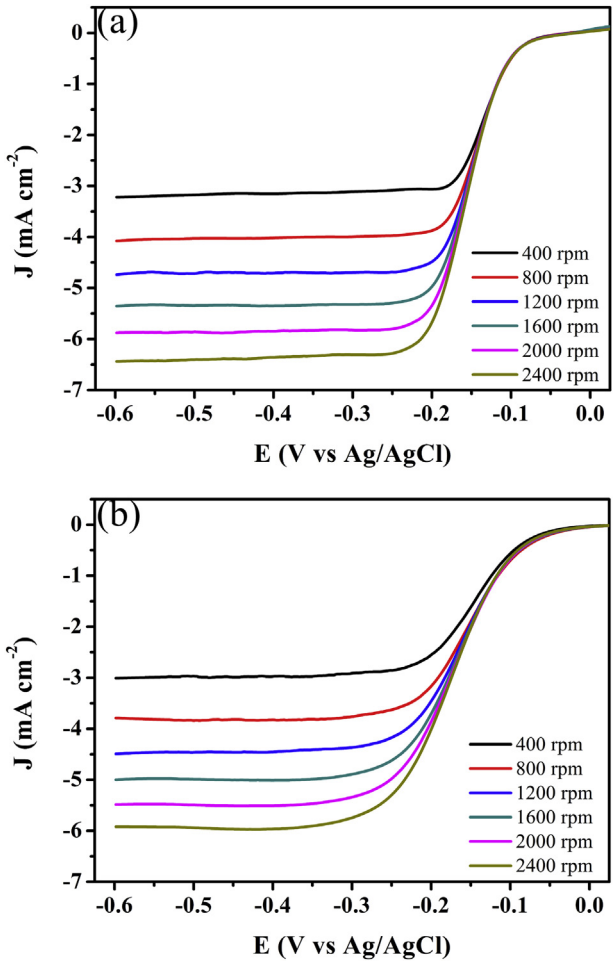

Fig. 5. RDE polarization curves at different rotation rates recorded in O_2-saturated 0.1 M KOH electrolyte (a) Co/N/rGO(NH_3) and (b) Pt/C(20%) electrodes, respectively; catalyst loading: 280 μg_{Cat} cm^{-2}_{geo} and scan rate: 5 mV s^{-1}. Electrolyte: O_2-saturated 0.1 M KOH, scan rate: 50 mV s^{-1}, and catalyst loading: 280 μg cm^{-2}.

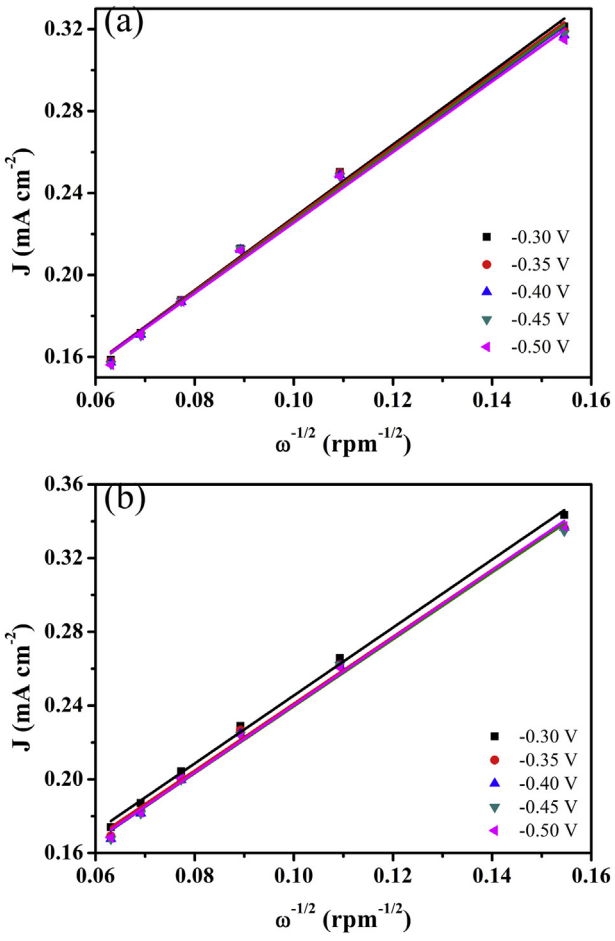

Fig. 6. Koutecky–Levich (K–L) plots for ORR on (a) Co/N/rGO(NH_3) and (b) Pt/C(20%) electrodes.

Ag/AgCl) as compared to other recently developed catalysts for ORR: triangular trinuclear Metal-N_4 complexes (E_{onset} = −140 mV vs. Ag/AgCl) [36], Ag-NPs/GC (E_{onset} = −280 mV vs. Ag/AgCl) and Ag-NCs/GC (E_{onset} = −130 mV vs. Ag/AgCl) [37], octabutylsulphonylphthalocyanine complexes of cobalt (CoOBSPc) supported on multi-walled carbon nanotube (MWCNT) (E_{onset} = −150 mV vs. Ag/AgCl) [38]. For our Co/N/rGO(NH_3) catalyst, E_{onset} is ∼10 mV lower than that for the commercial Pt/C(20%) catalyst (−100 mV). Moreover, the other key parameters characterize the catalytic activity for ORR, such as the half-wave potential ($E_{1/2}$) is ∼11 mV higher than that for the commercial Pt/C(20%) catalyst (−162 mV). These results demonstrate that Co/N/rGO(NH_3) catalyzes the ORR in facile manner under alkaline conditions.

The Co/N/rGO(NH_3) demonstrated more excellent ORR activity than Pt/C(20%) in this study. The enhanced ORR activity of Co/N/rGO(NH_3) might be attributed to the fact that carbon atoms in the GO matrix can potentially provide unique carbon chemistry, which may facilitate the formation of Co–N_x and N [39] groups (proposed as active site for ORR) using the synthesis method employed in this study.

Since durability is one of the major concerns in fuel cell technology, chronoamperometry was used to characterize the durability of the electrodes at a constant voltage of −026 V for 20,000 s in O_2-saturated aqueous solution of 0.1 M KOH at a rotation rate of 1600 rpm (Fig. 8). Remarkably, the corresponding current–time (*i*–*t*) chronoamperometric response of Co/N/rGO(NH_3) exhibits a very slow attenuation, and a high relative current of 86.5% still persists after 20,000 s. In contrast, Pt/C(20%) shows a gradual decrease with a current loss of approximately 73.3% measured after 20,000 s. This

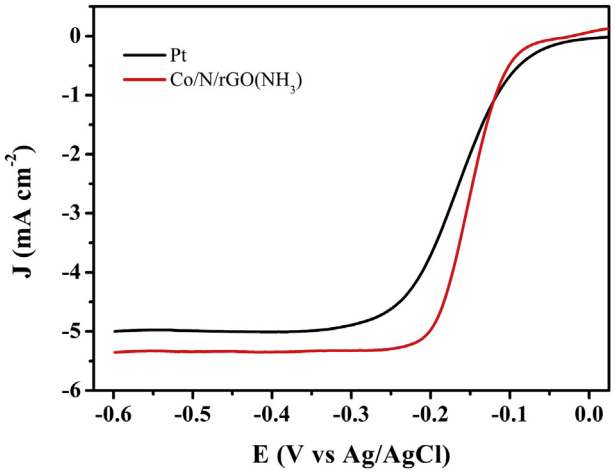

Fig. 7. RDE polarization curves of Co/N/rGO(NH_3) (red curve) and Pt/C(20%) (black curve) electrodes recorded in O_2-saturated 0.1 M KOH electrolyte at a rotating speed of 1600 rpm (For interpretation of the references to color in this figure legend, the reader is referred to the web version of this article.).

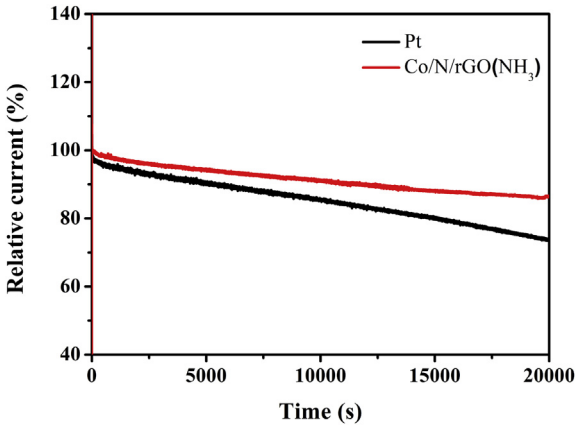

Fig. 8. Current–time (i–t) chronoamperometric responses for Co/N/rGO(NH_3) and Pt/C(20%) modified GC electrode at −0.26 V in O_2-saturated aqueous solution of 0.1 M KOH at a rotation rate of 1600 rpm.

result clearly suggests the better durability of Co/N/rGO(NH_3) compared with Pt/C(20%) catalyst.

4. Conclusions

We have successfully prepared a new graphene-based non-noble Co/N/rGO(NH_3) cathode catalyst using available PEI and $Co(NO_3)_2 \cdot 6H_2O$ precursors by first heat treatment in argon and secondly in ammonia. Both cobalt and ammonia have significant effects on improving the ORR catalytic activity observed in the Co/N/rGO(NH_3) hybrid. Due to the unique surface chemistry property, the introduction of rGO could facilitate to create active $Co-N_x$ sites and to improve the catalytic activity for ORR. XPS measurements reveal that the catalyst surface consists of ~6.23 at.% N (46% atom pyridinic N) and ~0.66 at.% Co relative to C. RDE testing also reveals a well-defined mass-transport-limited current that attests to high density of the ORR active sites. The onset potential and half-wave potential of oxygen reduction in 0.1 M KOH electrolyte can be as high as −0.110 V and −0.151 V, respectively. This graphene based catalyst exhibits a much higher selectivity and a much better stability for ORR, which may serve as a promising alternative to Pt/C(20%) catalysts for the ORR in alkaline solutions.

References

[1] W. Chen, D. Ny, S. Chen, Journal of Power Sources 195 (2010) 412–418.
[2] J.R.C. Salgado, E. Antolini, E.R. Gonzalez, Journal of Power Sources 138 (2004) 56–60.
[3] K. Gong, F. Du, Z. Xia, M. Durstock, L. Dai, Science 323 (2009) 760–764.
[4] Y. Liang, Y. Li, H. Wang, J. Zhou, J. Wang, T. Regier, H. Dai, Nature Materials 10 (2011) 780–786.
[5] I.V. Lightcap, T.H. Kosel, P.V. Kamat, Nano Letters 10 (2010) 577–583.
[6] A.K. Geim, K.S. Novoselov, Nature Materials 6 (2007) 183–191.
[7] A.R. Ranjbartoreh, B. Wang, X. Shen, G. Wang, Journal of Applied Physics 109 (2011) 014306.
[8] R. Kou, Y. Shao, D. Wang, M.H. Engelhard, J.H. Kwak, J. Wang, V.V. Viswanathan, C. Wang, Y. Lin, Y. Wang, I.A. Aksay, J. Liu, Electrochemistry Communications 11 (2009) 954–957.
[9] R. Bashyam, P. Zelenay, Nature 443 (2006) 63–66.
[10] M. Lefèvre, J.-P. Dodelet, Electrochimica Acta 48 (2003) 2749–2760.
[11] V. Nallathambi, J.-W. Lee, S.P. Kumaraguru, G. Wu, B.N. Popov, Journal of Power Sources 183 (2008) 34–42.
[12] G. Wu, Z. Chen, K. Artyushkova, F.H. Garzon, P. Zelenay, ECS Transactions 16 (2008) 159–170.
[13] L. Zhang, K. Lee, C.W.B. Bezerra, J. Zhang, J. Zhang, Electrochimica Acta 54 (2009) 6631–6636.
[14] H.-J. Zhang, Q.-Z. Jiang, L. Sun, X. Yuan, Z.-F. Ma, Electrochimica Acta 55 (2010) 1107–1112.
[15] F. Charreteur, F. Jaouen, S. Ruggeri, J.-P. Dodelet, Electrochimica Acta 53 (2008) 2925–2938.
[16] D.C. Marcano, D.V. Kosynkin, J.M. Berlin, A. Sinitskii, Z. Sun, A. Slesarev, L.B. Alemany, W. Lu, J.M. Tour, ACS Nano 4 (2010) 4806–4814.
[17] G. Wu, K.L. More, C.M. Johnston, P. Zelenay, Science 332 (2011) 443–447.
[18] T.E. Wood, Z. Tan, A.K. Schmoeckel, D. O'Neill, R. Atanasoski, Journal of Power Sources 178 (2008) 510–516.
[19] J.R. Pels, F. Kapteijn, J.A. Moulijn, Q. Zhu, K.M. Thomas, Carbon 33 (1995) 1641–1653.
[20] K. Artyushkova, S. Levendosky, P. Atanassov, J. Fulghum, Topics in Catalysis 46 (2007) 263–275.
[21] H.R. Byon, J. Suntivich, Y. Shao-Horn, Chemistry of Materials 23 (2011) 3421–3428.
[22] X. Li, H. Wang, J.T. Robinson, H. Sanchez, G. Diankov, H. Dai, Journal of the American Chemical Society 131 (2009) 15939–15944.
[23] J.-Y. Choi, R.S. Hsu, Z. Chen, The Journal of Physical Chemistry C 114 (2010) 8048–8053.
[24] D. Nguyen-Thanh, A.I. Frenkel, J. Wang, S. O'Brien, D.L. Akins, Applied Catalysis B: Environmental 105 (2011) 50–60.
[25] A. Morozan, P. Jegou, B. Jousselme, S. Palacin, Physical Chemistry Chemical Physics: PCCP 13 (2011) 21600–21607.
[26] S. Kundu, T.C. Nagaiah, W. Xia, Y. Wang, S.V. Dommele, J.H. Bitter, M. Santa, G. Grundmeier, M. Bron, W. Schuhmann, M. Muhler, The Journal of Physical Chemistry C 113 (2009) 14302–14310.
[27] M. Lefèvre, E. Proietti, F. Jaouen, J.-P. Dodelet, Science 324 (2009) 71–74.
[28] F. Jaouen, M. Lefèvre, J.-P. Dodelet, M. Cai, The Journal of Physical Chemistry B 110 (2006) 5553–5558.
[29] W.I. Choi, S.-H. Jhi, K. Kim, Y.-H. Kim, Physical Review B 81 (2010) 085441.
[30] S. Yang, L. Zhi, K. Tang, X. Feng, J. Maier, K. Müllen, Advanced Functional Materials 22 (2012) 3634–3640.
[31] S. Wang, E. Iyyamperumal, A. Roy, Y. Xue, D. Yu, L. Dai, Angewandte Chemie International Edition 50 (2011) 11756–11760.
[32] R. Liu, D. Wu, X. Feng, K. Müllen, Angewandte Chemie 122 (2010) 2619–2623.
[33] F. Cheng, Y. Su, J. Liang, Z. Tao, J. Chen, Chemistry of Materials 22 (2009) 898–905.
[34] Z. Chen, D. Higgins, Z. Chen, Carbon 48 (2010) 3057–3065.
[35] J. Maruyama, I. Abe, Electrochimica Acta 48 (2003) 1443–1450.
[36] R. Liu, C. von Malotki, L. Arnold, N. Koshino, H. Higashimura, M. Baumgarten, K. Mullen, Journal of the American Chemical Society 133 (2011) 10372–10375.
[37] Y. Lu, W. Chen, Journal of Power Sources 197 (2012) 107–110.
[38] S.A. Mamuru, K.I. Ozoemena, T. Fukuda, N. Kobayashi, T. Nyokong, Electrochimica Acta 55 (2010) 6367–6375.
[39] P. Matter, U. Ozkan, Catalysis Letters 109 (2006) 115–123.